Journal of Hydrology 617 (2023) 128978

Contents lists available at ScienceDirect

Journal of Hydrology

journal homepage: www.elsevier.com/locate/jhydrol

Research papers

Trends in soil frost formation in a warming maritime climate and the impacts on urban flood risk

Tarek Zaqout [a,*], Hrund Ólöf Andradóttir [a], Johanna Sörensen [b]

[a] Faculty of Civil and Environmental Engineering, University of Iceland, Hjarðarhagi 2-6, 107 Reykjavík, Iceland
[b] Division of Water Resources Engineering, Lund University, John Ericssons Väg 1, V-Hus, Lund, Sweden

ARTICLE INFO

This manuscript was handled by C. Corradini, Editor-in-Chief, with the assistance of Subashisa Dutta, Associate Editor

Keywords:
Climate change
Flooding
Rain on snow
Snowmelt
Frost
SHAW model

ABSTRACT

The most severe urban flooding in cold maritime climates is due to the co-action of long-duration rainfall, snowmelt, and soil frost. Increasing winter air temperature due to climate change is projected to change the magnitude and frequency of rain-on-snow (RoS) events and increase the number of freeze–thaw cycles and midwinter snowmelt. While daily rainfall records are readily available, less is known about the infiltration and frost formation within urban soils. Thus, there is uncertainty on how warming winter conditions may affect urban flood risk and the climate resilience of cities. The aim of this study was, therefore, to assess soil frost formation in the past 70 years in the maritime city of Reykjavík, Iceland (64° N, 21° W), and its co-action with runoff generation, and the potential implications on urban flood risk. To that end, the daily thermal and hydraulic conditions of the soil were simulated using the Simultaneous Heat and Water (SHAW) model dating back to 1949, calibrated based on hourly observations from 2007. Model simulations indicated that the minimum soil temperature at 10 cm depth has been warming at a rate of 0.015 °C/year in the past seven decades. Climate warming is also noted in a steady decline in frost depth and the duration of soil frost each winter (p-value < 0.05). However, the freezing season has shortened so that the timing of maximum frost coincides more with the timing of maximum RoS and snowmelt events. Furthermore, RoS events during frost have the capacity to produce larger runoff volumes than rainfall or snowmelt alone based on the joint frequency analysis of winter events using the copula method. This, combined with increasing volume during RoS events, suggests that winter floods may intensify in the next decades, which urges re-thinking urban stormwater management in cold climates.

1. Introduction

Soil frost is a widespread phenomenon affecting about 35 % of the earth's surface (Williams and Smith, 1989). Soil frost significantly alters the hydrological cycle, and surface and subsurface exchanges of water and energy (Shanley and Chalmers, 1999; Wang et al., 2009). Infiltration into frozen and partially frozen soils is reduced due to the presence of ice lenses (Granger et al., 2011; Khan et al., 2012; Slater et al., 1998; Wang et al., 2009). Soil frost paired with rain-on-snow (RoS) generated the greatest number of flooded properties in a cold maritime climate (Andradóttir et al., 2021). Additionally, frost formation is a key performance indicator for the hydrological performance of sustainable urban drainage systems (SUDS), which are increasingly adopted to integrate separate stormwater systems and increase cities' resilience to climate change (Zaqout et al., 2022; Zaqout and Andradóttir, 2021). Water infiltration into frozen soil is essential for understanding and managing the biological activity and nutrients in soils (Watanabe et al., 2013). Severe frost action can impair the development and even the existence of plants and, as such, is known to severely contribute to soil erosion and compromise land restoration efforts (Arnalds, 2015; Benninghoff, 1952).

The atmospheric-soil exchanges of heat and water, and hence soil frost formation, are governed by the surface conditions (snow and vegetation) and the physical properties of the underlying soil. Plant foliage influences the albedo and wind velocity profile near the soil surface, and hence the shortwave and turbulent heat exchanges; plant roots affect the soil porosity and stability (Flerchinger and Pierson, 1991; Zaqout et al., 2022). Snow is an effective insulator, and the absence or the late development of snowpacks leads to deeper and more persistent soil frost (Shanley and Chalmers, 1999; Stadler et al., 2000). The conductance of heat and water through the soil is affected by the grain size distribution, porosity, organic content, the presence of

* Corresponding author.
E-mail address: tarek@hi.is (T. Zaqout).

https://doi.org/10.1016/j.jhydrol.2022.128978
Received 30 May 2022; Received in revised form 30 September 2022; Accepted 7 December 2022
Available online 15 December 2022

Fig. 1. Greater capital area of Reykjavík, Iceland. Road infrastructure is marked as grey lines, the Atlantic Ocean and freshwater bodies in light blue, and the study sites as squares. The smaller map shows the location of Reykjavík's capital area in Iceland (For interpretation of the references to color in this figure legend, the reader is referred to the web version of this article).

Table 1
Summary of the soil physical properties and high-resolution weather and soil monitoring at the study sites.

		Urriðaholt	Reykjavík
Site	Elevation	42 m a.s.l.	52 m a.s.l.
	Distance to sea	2.8 km	2.5 km
	Land slope	3.3 %	0 %
	Surface cover	Grass	Grass
Soil	Soil type	Sandy loam	N/A
	Bulk density	1.46–1.93 g cm^{-3}	N/A
	Parameters	T_s & WC	T_s
	Depths	5, 15, 25, 35, 45 cm	10, 20, 50, 100 cm
	Period	Nov 2018–2022	Sep 2007–2019
	Resolution	10 min	1 h
Weather	Parameters	T_a, RH, Ps, W_s, W_d, P	T_a, RH, Ps, W_s, W_d, P, LW, SW
	Period	Feb 2019–2022	Sep 2007–2019
	Resolution	10 min	1 h

Notes: T_s = soil temperature (°C), WC = water content, RH = relative humidity (%), P_s = atmospheric pressure (hPa), W_s = wind speed (m/s), W_d = wind direction, P = Precipitation (mm), L/SW = long/short wave radiation (W/m^2).

macropores and cracks, and the water content of the soil at the onset of freezing (Stähli et al., 1999). Specifically, dry soils have been found to maintain infiltration even when frozen, while saturated soils promote concrete frost formation (Granger et al., 2011; Kane, 1980).

Coastal cold regions are subjected to intermittent midwinter snowmelt, RoS events, and freeze–thaw cycles (Andradóttir et al., 2021; Muthanna et al., 2008). The repeated supply of near-freezing meltwater, together with the lack of the thermal insulation provided by a continuous snow cover, results in an excessive wetting of the soil, rendering it susceptible to frequent freezing and thawing (Zaqout et al., 2022; Zaqout and Andradóttir, 2021). Frequent freeze–thaw cycles (FTCs) negatively affect soil ecosystem diversity and productivity because they cause changes in soil physical properties, lead to soil deformation, and affect water movement (Fouli et al., 2013). Liquid-solid phase changes alter the soil's hydraulic and thermal properties significantly (Lundin, 1990; Watanabe and Kugisaki, 2017; Zheng et al., 2021). Thus, to fully understand frost formation in a cold maritime climate undergoing frequent freeze–thaw requires the monitoring of both water content and soil temperature. Alternatively, coupled modeling of heat and water transfer through the snow, vegetation, and soil profiles can be used. Several numerical models of soil freezing and thawing have been developed for agricultural, forestry, ecological, and civil engineering applications (e.g., Flerchinger and Saxton, 1989a; Flerchinger and Saxton, 1989b; Guymon and Luthin, 1974; Hansson et al., 2004; Jansson and Karlberg, 2004; Šimůnek et al., 2016). However, most studies on soil freezing and thawing used data from laboratory experiments to calibrate and validate the models (He et al., 2015; Zheng et al., 2021), which may not be representative of the temporal and spatial variations in atmospheric forcing, soil layering, vegetation covers in the field (Zheng et al., 2021).

Assessing flood risks in urban areas is difficult due to the heterogeneous nature of urban catchments and the complex interactions between rain, snow, and soil frost (Andradóttir et al., 2021; Moghadas et al., 2018). In recent years, joint probability theories have been adopted to analyze flood risk resulting from two or more hydrologic variables (Lian et al., 2013; Sörensen and Bengtsson, 2014; Zellou and Rahali, 2019), the most famous of which is the copula probability model (Chen, 2019; Nelsen, 2007). Introduced by Sklar (1959), the method involves expressing a multivariate joint cumulative distribution function in terms of univariate marginal distribution functions and describing the dependence between the variables with copula functions (Salvadori and De Michele, 2007).

With more wet and warm winters, precipitation falls more in liquid form. Midwinter melt and RoS events have been found to become more frequent (Garvelmann et al., 2015; Surfleet and Tullos, 2013; Wever et al., 2014; Würzer and Jonas, 2018) and RoS events more voluminous (Andradóttir et al., 2021). Moreover, the number of freeze–thaw cycles has been increasing in mountainous regions (Garvelmann et al., 2015; Würzer et al., 2016). Frequent RoS, snowmelt, frost formation, and infiltration in frozen ground are highly interlinked processes and less understood than during continuous snow cover (Wever et al., 2014). While soil frost is a key indicator of urban flooding, it is rarely considered when planning urban drainage systems (Bengtsson and Westerström, 1992; Caraco and Claytor, 1997; Maksimovic et al., 2000). The lack of routine monitoring of soil is also a limiting factor for understanding urban flood risk and how the urban flood risk may change with climate change. Therefore, the goal of this research was, on the one hand, to improve the understanding of soil frost formation in an area undergoing frequent freeze–thaw cycles and RoS events by means of numerical modeling. On the other hand, the study aims to assess the impacts of climate change on winter flood risk by analyzing the joint probability and timing of winter flood indicators (i.e., rainfall, snowmelt, and RoS events) in the presence of soil frost. Lastly, the implications of the research findings on urban flood risk and stormwater management are discussed in the context of the need for more climate-resilient cities, as stipulated by the United Nations (Sustainable Development Goal No. 11).

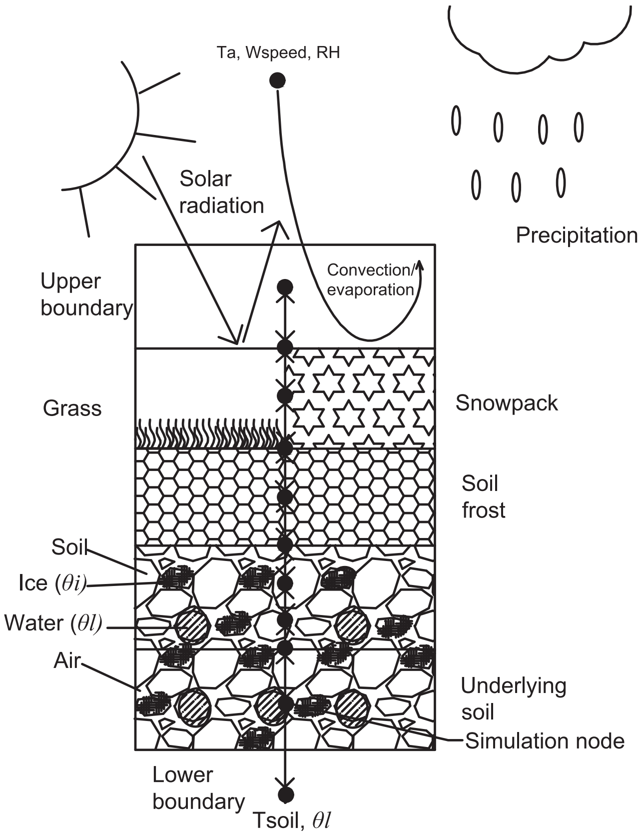

Fig. 2. Physical system described by the SHAW model showing the upper (energy budget at the surface) and lower boundary, snowpack and soil frost on the right, the vegetation cover, and the underlying soil constituents on the left.

2. Materials and methods

2.1. Study site and data collection

The capital region of Reykjavík (230,000; 1000 km^2) includes six municipalities sited within a few kilometers from the coastline in the southwestern corner of Iceland (Fig. 1). The local climate is heavily influenced by the Gulf Stream, with cool summers and mild winters with temperatures fluctuating around the freezing point (Einarsson, 1984). Soil frost rarely extends beyond 20 cm depth (Petersen, 2018). Precipitation tends to be frequent and mild (213 rainy days totaling approx. 1000 mm per annum; Ólafsson et al. (2007)). Precipitation falls mostly at high winds with the forward passage of cyclones from the southwest, which prevail especially in winter (Einarsson, 1984). The most severe urban flood events in Reykjavík were associated with the co-action of rain, snow, and soil frost (Andradóttir et al., 2021).

Data from two sites located 6 km apart were obtained for the purpose of the study (Fig. 1). Both sites were located in open grassed-covered areas, 40–50 (m a.s.l.) and at <3 km distance from the ocean (Table 1).

2.1.1. Urriðaholt site

Hourly weather and soil temperature data were compiled from the high resolution (10 min) monitoring program in the residential neighborhood Urriðaholt in Garðabær, Iceland (64° 4′18.46″ N, 21° 54′37.11″ W) as described in Zaqout et al. (2022). The neighborhood was built with a large network of sustainable urban drainage systems (SUDS) to safeguard the quantity and quality of water entering Urriðavatn pond. Soil temperature and water content were monitored at 5, 15, 25, 35, and 45 cm depths within a grass swale for the period of November 2018 until 2022 (Table 1).

Soil physical characteristics at different horizons, such as particle size distribution and bulk density, were measured in the laboratory using collected samples from the study swale. The soil was classified as sandy loam with 15–20 % gravel, 75–82 % sand, and 2.5–4 % fines (clay and silt). Saturated soil water content and field capacity were estimated from observed soil water content measured using water content reflectometers. Saturated hydraulic conductivity was estimated based on typical values for the corresponding soil textural class, cross-checked with single-ring infiltration measurements at the study site. More details on the soil monitoring program are available in Zaqout and Andradóttir (2021) and Zaqout et al. (2022).

2.1.2. Reykjavík site

Daily weather and snow depth measurements were available at the Reykjavík station for the period of 1949–2018, which was measured at the headquarters of the Icelandic Meteorological Office (IMO) located in Bústaðavegur 7, Reykjavík (64° 07′39.1″ N, 21° 54′08.5″ W). Hourly soil temperature, weather, longwave and shortwave radiation data were also available from the Reykjavík station for the period of 2007–2019 (Table 1).

2.2. Numerical modeling

2.2.1. SHAW model description

The Simultaneous Heat and Water (SHAW) model (Flerchinger and Saxton, 1989a; Flerchinger and Saxton, 1989b), is an open-source model, which has been widely used to simulate soil temperature and frost (Kahimba et al., 2009). The model is a physically-based, finite-difference, coupled heat, water, and solute transfer. It consists of a vertical, one-dimensional profile extending from the energy exchange between the atmosphere and the surface, the vegetation canopy, the snow cover if present, and to a certain depth within the soil (Fig. 2). While several models assume soil freezing has the same effect as drying soil, the SHAW model takes into account the reduction in soil porosity in subzero conditions due to the presence of ice-filled pores at which hydraulic conductivity is reduced linearly with ice content (Kahimba et al., 2009; Flerchinger, 2000). The water balance is expressed as (Flerchinger and Saxton, 1989a):

$$\frac{\partial\theta_l}{\partial t}+\frac{\rho_i}{\rho_l}\frac{\partial\theta_i}{\partial t}=\frac{\partial}{\partial Z}\left[K\left(\frac{\partial\Psi}{\partial Z}\right)+1\right]+\frac{1}{\rho_l}\frac{\partial q_v}{\partial Z} \tag{1}$$

where t is the time (s), θ_l is the liquid volumetric water content (m^3 m^{-3}), θ_i is the frozen volumetric water content (m^3 m^{-3}), ρ_l is the liquid water density (kg m^{-3}), ρ_i is the ice density (kg m^{-3}), K is the hydraulic conductivity (m s^{-1}), Ψ is the soil water matric potential (m H_2O), q_v is the vapor water flux (m s^{-1}), and Z is the depth (m).

The relationship between matric potential, Ψ, liquid water content, θ_l, and hydraulic conductivity, K, is expressed by a set of equations that govern the water movements in the soil (Campbell, 1974).

$$\Psi=\Psi_e\left(\frac{\theta_l}{\theta_s}\right)^{-b} \tag{2}$$

$$K=K_s\left(\frac{\Psi_e}{\Psi}\right)^{2+\left(\frac{3}{b}\right)}=K_s\left(\frac{\theta_l}{\theta_s}\right)^{2b+3} \tag{3}$$

here, θ_s is the saturated water content (m^3 m^{-3}), Ψ_e is the air entry potential (m H_2O), and b is the pore size distribution index, K_s is the saturated hydraulic conductivity (m s^{-1}). Once frost is developed, the capillary suction acts to pull water from the unfrozen soil upwards towards the freezing front. This equation describing the relationship between matric potential Ψ, and soil temperature T (°C) is as follows (Fuchs et al., 1978):

$$\Psi=\frac{L_f}{g}\left(\frac{T}{T+273.16}\right) \tag{4}$$

Table 2
Soil physical and hydraulic characteristics used as input parameters for the SHAW model.

Study site	Urriðaholt					Reykjavík			
Bottom depth of soil horizon [cm]	5	15	25	35	45	10	20	50	100
Clay [%]	15	17	16	3	3	15	17	16	7
Sand [%]	75	70	70	95	96	75	70	70	78
Silt [%]	10	13	14	2	1	10	13	14	15
Organic matter [%]	25	22	20	18	17	25	22	20	18
Bulk density [g/cm^3]	1.02	0.8	0.9	1	1.2	1.02	0.8	0.9	1
Saturated water content [m^3/m^3]	0.54	0.44	0.43	0.33	0.32	0.54	0.41	0.4	0.33
Saturated conductivity [cm/h]	10	9	9	10	12	0.5	0.4	0.4	0.4
Air entry potential [bars]	0.001	0.004	0.004	0.003	0.002	0.001	0.003	0.004	0.003
Pore size index	6.3	9.9	9.8	9.9	9.89	6.3	9	9	9.9

where g is the gravitational acceleration (m s^{-2}), L_f is the latent heat of fusion (J m^{-3}). The ice content θ_i can be determined as the difference between the total water content and the maximum liquid water content.

The governing one-dimensional energy equation, which includes soil temperature, freezing and thawing, and conductive and convective heat transfer of liquid and vapor, is described by Flerchinger and Saxton (1989a)

$$C_s\frac{\partial T}{\partial t}-\rho_i L_f\frac{\partial\theta_i}{\partial t}=\frac{\partial}{\partial Z}\left(\lambda_s\frac{\partial T}{\partial Z}\right)-\rho_l c_l\frac{\partial(q_l T)}{\partial Z}-L_v\left(\frac{\partial q_v}{\partial Z}+\frac{\partial\rho_v}{\partial t}\right) \tag{5}$$

where C_s is the volumetric heat capacity of the soil (J m^{-3} °C^{-1}), λ_s is the soil thermal conductivity (W m^{-1} °C^{-1}), and c_l is the specific heat of liquid water (J kg^{-1} °C^{-1}). The heat capacity of the soil is based on summing the heat capacities and densities of the different soil constituents (i.e., minerals, organic matter, water, ice, and air) following the method developed by de Vries (1963) and modified for frozen soils by Penner (1970)

$$C_s=\sum\rho_j c_j\theta_j \tag{6}$$

where ρ_j, c_j, and θ_j are the density, specific heat capacity, and the volumetric fraction of the j^{th} soil constituent. The thermal conductivity is expressed as

$$\lambda_s=\frac{\sum m_j\lambda_j\theta_j}{\sum m_j\theta_j} \tag{7}$$

where m_j, λ_j, and θ_j are the weighting factor, thermal conductivity, and the volumetric fraction of the j^{th} soil constituent (Flerchinger, 2000).

The surface boundary condition is determined by the energy balance on the surface as follows:

$$R_n+H_{sf}+L_vE_{sf}+G=0 \tag{8}$$

where R_n is the net radiation (W m^{-2}), H_{sf} is sensible heat flux (W m^{-2}), E_{sf} is the evaporation rate (m s^{-1}), and G is the ground conduction flux (W m^{-2}). Further description of the physical processes used by the model is given by Flerchinger (2000), Flerchinger and Saxton (1989a), and Flerchinger and Saxton (1989b).

2.2.2. Input parameters and initial conditions

At the Urriðaholt study site, the hourly averages of weather conditions constructed from the 10-minute observations at the study site were used as inputs for the model and soil temperature and moisture content were used as initial values (Table 1). Hourly incoming shortwave radiation was used from the Reykjavík station no.1 for the same period (IMO, 2022a). The dataset was split into two; a calibration period from November 2018 to August 2020, and a validation period from August 2020 to May 2022. The soil physical properties determined from the soil samples were used for the initial runs and adjusted to calibrate the model (Table 2). In Reykjavík, the model was first calibrated and tested using the available hourly soil temperature data from 2007 until 2019 (Table 1). Soil physical and hydraulic characteristics were manually adjusted by trial-and-error, starting with measured soil properties in Urriðaholt as a basis (Table 2). The model was then run using the daily weather observations (i.e., air temperature, relative humidity, precipitation, and wind speed) measured from midnight to midnight for the targeted period of 1949 to 2018 (IMO, 2020b).

Historical solar radiation was estimated based on the potential extraterrestrial solar radiation (S_o, W m^{-2}) based on latitude and day of year. Following the approach outlined in Bras (1990), the clear sky solar radiation, S_c, was estimated as

$$\frac{S_c}{S_o}=\exp(-n\alpha_1 m) \tag{9}$$

where a turbidity factor of $n=3$ was chosen to represent the clean urban area, α_1 is the molecular scattering coefficient, and the optical air mass, m, approximated by the cosecant ($1/\sin\alpha$) of the solar altitude α. The net radiation incoming radiation was estimated as

$$\frac{S_s'}{S_c}=1-0.65N^2 \tag{10}$$

where N is measured diurnal cloud cover, converted from oktas to a ratio from 0 to 1. The reconstructed daily shortwave radiation agreed well with observations from 2007 to 2018 ($R^2=0.9$, RMSE = 33 W/m^2; Fig. A.1).

2.2.3. Model performance evaluation

The model prediction ability was primarily assessed based on soil temperature and secondarily on the basis of soil water content. Two performance metrics were used. The linear correlation coefficient (R^2) was calculated to test how well seasonal and synoptic changes were represented in the model. In addition, the root mean square error (RMSE) was calculated to assess the average deviation between the observed and simulated value at each time step.

2.3. Data analyses

2.3.1. Soil frost statistics and trends

The most relevant model outputs to soil frost were soil frost depth, soil temperature, and ice content for each soil layer (m^3 m^{-3}). SHAW model calculates frost depth via linear interpolation of ice content in the deepest layer with frost. A soil layer can have a sub-freezing temperature but will not be considered frozen unless ice is present. For each calendar year, the number of frost days and days with continuous frost were determined. A freeze–thaw cycle (FTC) was determined based on the presence of frost in the form of ice content. The model resolved frost in the top centimeters of the soil and predicted more FTCs than observed at selected depths, e.g., at 10 cm (see Andradóttir et al., 2021).

Trends were assessed using the Mann-Kendall test (Kendall, 1948; Mann, 1945) and the significance of the slope using the Theil-Sen method (Sen, 1968; Theil, 1950). These methods were chosen due to their simplicity because they are non-parametric (the data does not need

Table 3
Bivariate Archimedean copula families and their functions and generators. The marginal (univariate) distributions are u_1 and u_2, and θ is the estimated bivariate copula parameter.

Copula	C (u_1, u_2)	Generator	Parameter
Joe (1997)	$1-\left[(1-u_1)^{\theta}+(1-u_2)^{\theta}-(1-u_1)^{\theta}(1-u_2)^{\theta}\right]^{\frac{1}{\theta}}$	$\varphi(t) = -ln\left[1-(1-t)^{\theta}\right]$	$\theta \in [1,\infty)$
Clayton (1978)	$(u_1^{-\theta}+u_2^{-\theta}-1)^{-\frac{1}{\theta}}$	$\varphi(t) = t^{-\theta}-1$	$\theta \in (0,\infty)$
Gumbel (1960)	$exp\left\{-\left[(-\ln(u_1))^{\theta}+(-ln(u_2))^{\theta}\right]^{\frac{1}{\theta}}\right\}$	$\varphi(t) = (-lnt)^{\theta}$	$\theta \in [1,\infty)$
Frank (1979)	$-\frac{1}{\theta}ln\left[1+\frac{(e^{-\theta u1}-1)(e^{-\theta u2}-1)}{e^{-\theta}-1}\right]$	$-ln\left(\frac{e^{-\theta t}-1}{e^{-\theta}-1}\right)$	$\theta \in R\backslash\{0\}$

Table 4
The SHAW model prediction performance of hourly soil temperature and water content in the grass swale in Urriðaholt 2018–2022 and Reykjavík 2007–2018. The range represents varying soil depth or variations between winters.

Site			Calibration		Validation	
			R^2	RMSE	R^2	RMSE
Reykjavík	T_s	All seasons	0.91–0.92	0.98–1.64	–	–
		Winters	0.30*–0.94	0.82–2.53*		
Urriðaholt	T_s	All seasons	0.98–0.99	0.66–0.89	0.97–0.98	0.71–0.93
	T_s	Winter 1, 2	0.71–0.94	0.40–1.08	–	–
	T_s	Winter 3, 4	–	–	0.66–0.88	0.66–0.99
	WC	All seasons	0.1–0.43	0.02–0.06	0.2–0.44	0.01–0.06

Notes: * Greater deviations were found for the last three years. Winter 1, 2, 3, and 4 refer to the four winters between 2018 and 2022.

to conform with any particular distribution), they allow for missing data, and can be used for small datasets ($n < 40$; Gilbert, 1987). A significant trend is considered for a 95 % confidence level ($\alpha = 0.05$).

2.3.2. Co-probability of liquid water and frost

The approach to understanding the co-action of hydrological inputs and soil frost was to estimate the joint probability of occurrence of two winter hydrological events. The combined daily precipitation and snow depth measurements at 9 A.M., annual maximum rainfall, snowmelt, and rain-on-snow in the presence of soil frost were calculated. Rainfall was distinguished from snowfall based on a temperature threshold, T_{RH} (°C), that incorporated relative humidity, RH (%), following the method presented by Feiccabrino et al. (2015)

$$T_{RH} = 0.75 + 0.085(100 - RH) \tag{11}$$

With this definition, daily precipitation was classified either as dry or wet, when in some instances, it can take both forms. Snowmelt was defined based on the reduction of snow depth, ΔSD, converted to snow water equivalent assuming a snow density, ρ_s, of 200 kg m^{-3}, in relation to a water density, ρ_w, of 1000 kg m^{-3}. If precipitation was recorded together with a reduction in snow depth, it was assumed to be rainfall. The magnitude of RoS was taken as the sum of the rain and liquid snowmelt volume (mm) estimated from measured snow depth (in cm) as presented in (Andradóttir et al., 2021)

$$RoS = P + snowmelt = P + \left(\frac{\rho_s}{\rho_w} \times \Delta SD \times 10\right) \tag{12}$$

Each of the annual daily maximum datasets was fitted to a distribution using the maximum likelihood method, and the goodness of fit was assessed using the Kolmogorov-Smirnov, Cramer-von Mises, and Anderson-Darling tests. Then, the distribution with the lowest Akaike (AIC) and Bayesian Information Criteria (BIC) was chosen. As such, maximum snowmelt during frost was fitted to the lognormal distribution, maximum frost during snowmelt to the Weibull distribution, maximum rainfall during frost to the lognormal distribution, and maximum frost during rainfall to the Weibull distribution. Maximum RoS during frost, and maximum frost during RoS were both fitted to the Weibull distribution (Table A.2). The return periods were then derived for each of the co-acting hydrological variables (Chow et al., 1988).

The copula method was used to estimate the joint distribution C ($F_x(x)$, $F_y(y)$) = C (u_1, u_2) of two dependent variables based on their marginal distributions of the annual maximum values fitted to a theoretical distribution $F_x(x) = u_1$ and $F_y(y) = u_2$ (Chen, 2019; Lian et al., 2013; Zellou and Rahali, 2019). The four Archimedean copulas most widely used for hydrological analyses due to their simplicity (Nelsen, 2007) were tested (Table 3). The three pairs of winter flood-inducing hydrological variables (i.e., maximum snowmelt during frost, rainfall during frost, and RoS during frost) were then fitted to one of the bivariate Archimedean copulas (i.e., Joe, Clayton, Gumbel, and Frank) using the maximum likelihood method. The bivariate copula family that best fits the pair was chosen based on the highest log-likelihood and lowest AIC and BIC (Zellou and Rahali, 2019). Two sets were modeled using the Clayton copula, and RoS during frost was fitted using the Frank copula (Table A.1).

The probabilities of the joint occurrence of annual maxima for the period of 1949–2018 were estimated based on the joint cumulative distribution function (CDF). Furthermore, the bivariate joint return periods for the annual maxima were derived as the inverse of the probability of both events occurring simultaneously, defined as the AND operator. The joint probability of exceedance for two hydrological events was calculated following Lian et al. (2013) and Zellou and Rahali (2019) as:

$$P((X > x) \cap (Y > y)) = 1 - F(x) - F(y) + F(x, y) \tag{13}$$

where P ((X > x) ∩ (Y > y)) is the probability of both X and Y exceeding a certain threshold.

3. Results

3.1. Model simulation performance

3.1.1. Soil temperature

The SHAW model accurately predicted the hourly, daily, and seasonal changes in soil temperature at various depths within the top 1 m of soil at both sites during all seasons, as reflected in $R^2 > 0.91$ and RMSE = 0.66–1.64 °C (Table 4). The model performed slightly better at

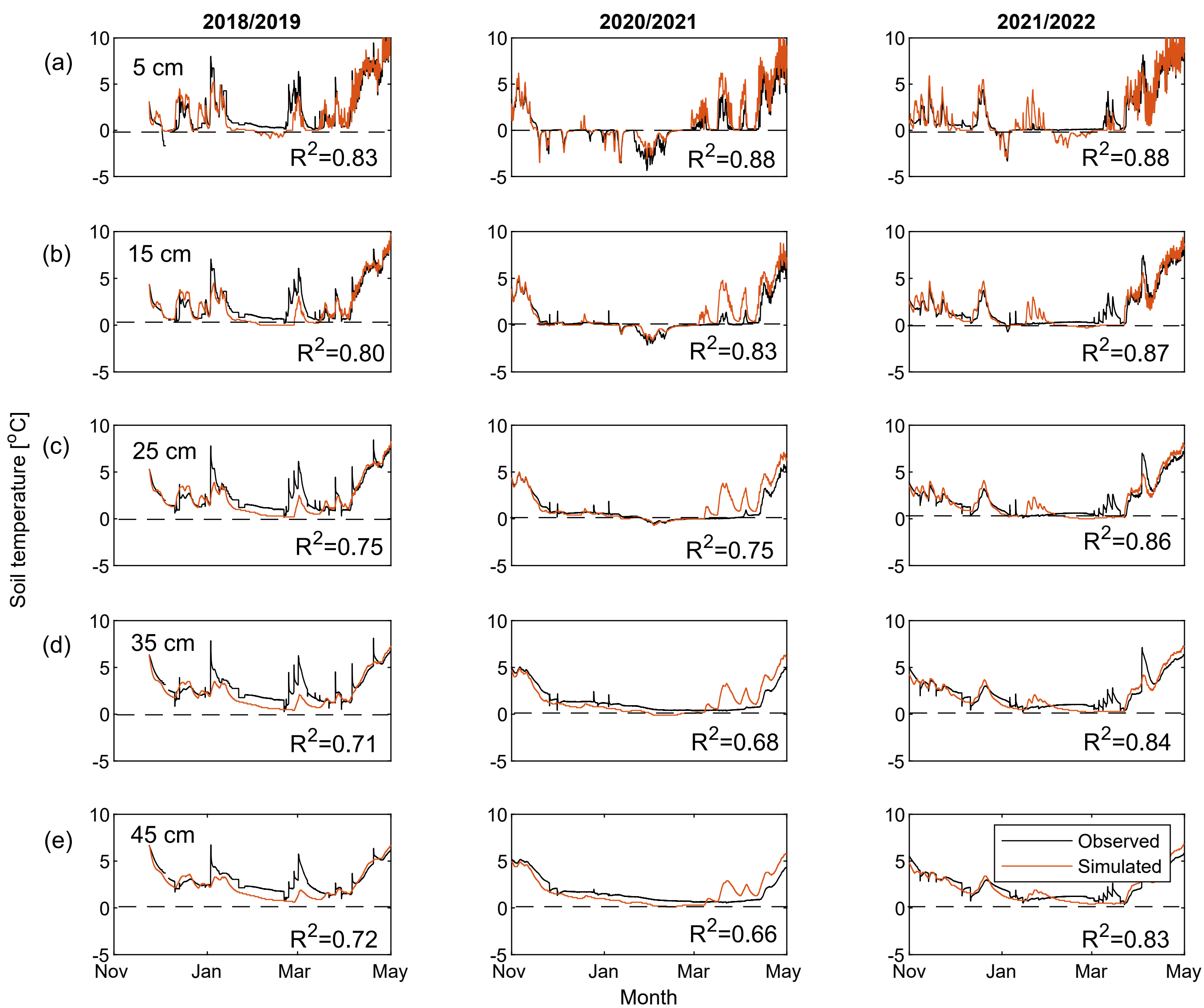

Fig. 3. Observed and simulated soil temperature in the grass swale in Urriðaholt during winter 1 (2018/2019; left panels), winter 3 (2020/2021; middle panels), and winter 4 (2021/2022; right panels) at a) 5 cm depth, b) 15 cm, c) 25 cm, d) 35 cm, and e) 45 cm.

Urriðaholt, where soil properties were tested in the laboratory and the field, than at the Reykjavík site, where the soil properties were not measured. In the Urriðaholt site, the model performed equally well during the calibration period (until August 3, 2020) and validation period (starting August 4, 2020). While the model performance dropped during winters at both sites (lower R^2 and RMSE, Table 4), the timing of frost formation and thawing was well captured within the top 25 cm of the soil that is most susceptible to frost (Fig. 3a–c). Hence, for urban hydrology applications, the model predicts very well repeated freeze–thaw in the top 25 cm of soil. The model performance was slightly lower in the bottom layers. Lastly, the model was less reliable in capturing temperature peaks during the winter of 2019/2020, when synthetic runoff experiments were conducted in the grass swales (Zaqout and Andradóttir, 2021; not shown in Fig. 3).

3.1.2. *Soil liquid moisture content and frost depth*

The simulated moisture content deviated considerably from observed values at Urriðaholt (Table 4). For the entire monitoring period, the model's performance was relatively more accurate for the validation period than the calibration (R^2 = 0.1–0.43 vs 0.2–0.44). The simulated values were worse during winter when the model failed to capture sharp increases during rainfall. It did, however, capture relatively well the reduction in liquid moisture content resulting from soil freezing. Most importantly, the model accurately predicted soil frost formation and frost depth during four winters with very different frost conditions (Fig. 4). During the first winter (2018/2019), frost was only observed at the topsoil horizon (5 cm), represented by negative soil temperature and a reduction in the liquid moisture content due to the phase change (heavy horizontal line in Fig. 4). The model, however, predicted the frost depth to have reached down to a 12 cm depth. This was also shown in the simulated ice content by the model as ice developed at the 5-cm simulation depth ($\theta_i = 0.24$) and slightly at 15 cm depth ($\theta_i = 0.07$). During the second winter, more occurrences of soil frost compared to the first winter were predicted and frost persisted longer (Fig. 4). Still, the maximum frost depth similarly did not extend beyond the 15-cm soil horizon, which was also consistent with field observations (Zaqout et al., 2022; Zaqout and Andradóttir, 2021). However, the simulated ice content was almost double of that during the preceding winter ($\theta_i = 0.41$ at 5 cm depth). This indicated that the topsoil horizon was almost completely frozen with few soil pores available for infiltration ($\theta_{max} = 0.54$ at 5 cm depth). The most severe freezing reaching down to 31 cm depth was predicted during the third winter, consistent with frost observed at 25 cm depth. The maximum ice content at 5 cm was similar to the one during the preceding winter ($\theta_i =$

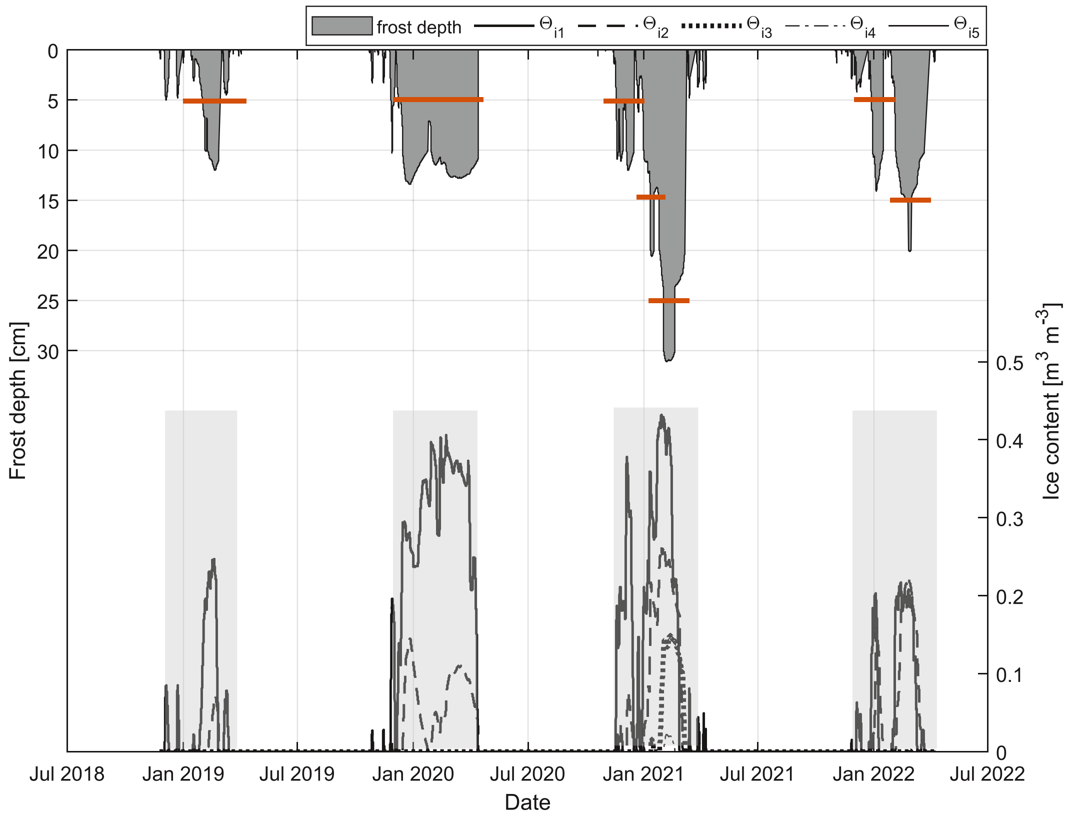

Fig. 4. Total simulated frost depth and ice content at 5, 15, 25, 35, and 45 cm depths (θ_{i1}–θ_{i5}) in the grass swale in Urriðaholt in winters between 2018 and 2022. Solid orange horizontal lines are the observed maximum frost depth (measured at 5, 15, 25, 35, and 45 cm depth).

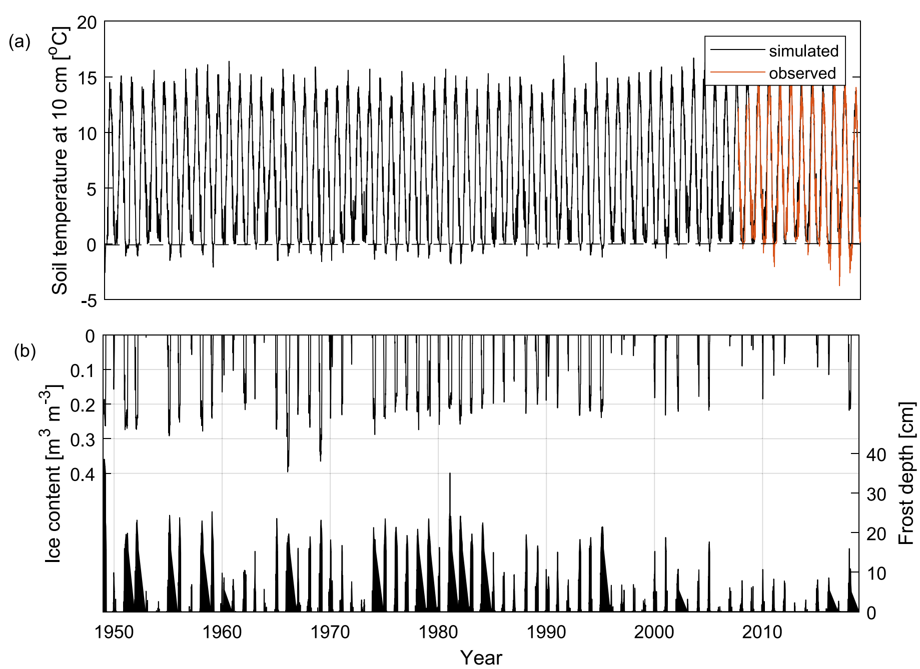

Fig. 5. a) simulated diurnal soil temperature in reykjavík from 1949 to 2018 and observed (2007–2018) at 10 cm, b) time evolution of soil frost depth and ice content (θi) at 10 cm depth in Reykjavík from simulations from 1949 to 2018.

0.43). All the layers, except the one at 45 cm, developed frost represented in the predicted ice content (θ_i = 0.26, 0.15, and 0.02) for the second, third, and fourth layers, respectively. During the fourth and last winter, the soil was frozen down to a maximum of 20 cm, and the maximum ice content was 0.22 at 5 cm depth as well as 15 cm, consistent with maximum frost depth observed at the 15 cm horizon. Overall, the model gave considerable novel insights beyond the observations at finer intervals.

Table 5
Summary statistics of predicted soil frost in Reykjavík for 1949–2018.

	Max.	Min.	Avg. ± Std.
T_{soil} [°C] at 10 cm	17.5	−2.6	6.1 ± 5.2
Frost depth [cm]	39	0.1	9.9 ± 8.1
No. days with soil frost	153	26	85.8 ± 29.7
No. days with continuous frost	158	4.0	65.6 ± 40.8
No. of soil FTC	8.0	1.0	3.65 ± 1.95

3.2. Daily soil frost predictions 1949–2018

3.2.1. Summary statistics

Daily soil temperature and moisture content at 10, 20, and 50 cm depths, frost, and snow depth were simulated using the calibrated SHAW model and historical weather data at Reykjavík dating back to 1949. Selected time series are presented in Fig. 5, and top-level statistics are summarized in Table 5. The model predicted some increase in winter soil temperature (Fig. 5a). The lowest soil temperature at the surface (−3.7 °C) and 10 cm (−2.6 °C) was simulated for the winter of 1949. However, the model overestimated the measured soil temperature in the last three winters (2015–2018; RMSE = 0.82–2.5, R^2 = 0.3–0.94) while correctly identifying the timing of frost. Frost depth and ice content was seen to decrease in the past 70 years (Fig. 5b). The maximum number of days with soil frost in any given calendar year was 153 days (Table 5), which was in 1951. Meanwhile, the minimum number of frost days was 26 days in 1987 and the shortest period of continuous frost lasted for only 4 days, also in 1987. The average number of freeze–thaw cycles in a year is 3.65, and the maximum was 8 cycles, occurring both in 1965 and 1971.

3.2.2. Sensitivity analyses

A sensitivity analysis was conducted using several selected parameters, both at the surface and within the soil profile, as well as selected meteorological inputs (Table 6). Common soil textural classes according to the USDA (1987) and saturated hydraulic conductivity were tested. Uncertainty regarding precipitation depth in dry form (snowfall) was also tested using the wind correction method presented by Crochet et al. (2007). The model predictions were consistent in terms of maximum predicted frost depth, no. of frost days, and FTCs, as well as soil temperature (RMSE = 1.51–2.11; R^2 = 0.91–0.93). The model was most sensitive to changes in vegetation cover. Specifically, if the ground was considered bare, the RMSE increased substantially (2.11 °C). The model was somewhat sensitive to soil texture class, reflected in a slightly lower RMSE and number of frost days if the soil was considered to contain more fines. The model was not sensitive to hydraulic conductivity or precipitation in dry form (snowfall).

3.2.3. Trends

The Mann-Kendall and Sen's slope tests suggest that soil frost depth decreased significantly (p-value < 0.05) in the 70 years analyzed in this study (Fig. 6a and Table 7). Similarly, the total number of days with soil frost near the surface has almost halved during these seven decades, from 108 to 62 days (Fig. 6b). This trend is even greater when considering the number of soil frost days at 15 cm depth (Table 7). Projecting the simulations forward, soil frost may rarely reach 15 cm in another two decades. Soil frost has also become less persistent, as the number of days with continuous soil frost decreased significantly (p-value < 0.05; Fig. 6c and Table 7). This suggests that the instances of intermittent formation of soil frost have increased during winter, which was reflected in the increase, however insignificantly, in the number of freeze–thaw cycles over the studied 70 years. The increase in the frequency of intermittent frost can also be seen in the significant increase in the minimum soil temperature at 10 cm depth in Reykjavík for the simulation period of 1949 to 2018 (Fig. 6d).

3.3. Co-probability of soil frost and runoff generation

The maximum RoS volume during frost and maximum frost during RoS were both found to fit the Weibull distribution. The univariate return period and event depth (i.e., RoS in mm, and frost in cm) were derived (Table 8). The joint cumulative distribution function of RoS and frost was then calculated using the Frank copula (Table 3). The probability of simultaneous occurrence was obtained using Eq. (13). The probability of two hydrological events occurring simultaneously is considerably lower than the probability of only one occurring at a time, but the severity of such events is higher. For instance, a 5-year RoS event (30 mm) occurring simultaneously with a 2-year frost depth (11 cm) has a bivariate return period of approximately 9 years (Table 8). A 30-mm event if taken into consideration separately, it might be classified as moderate event. However, if it occurred simultaneously with soil frost, it could lead to substantial runoff and flooding. Furthermore, a 2-year RoS event (20 mm) and a 2-year frost depth (11 cm) have a probability of co-occurring with a return period of <4 years (27 %). Such event can be considered frequent and is known to produce substantial water-related insurance claims in Reykjavík (Andradóttir et al., 2021).

Among the three tested sets (i.e., snowmelt & frost, rainfall & frost, and RoS & frost), the RoS volume during frost was found to be the highest (Fig. 7). Extreme snowmelt events resulting in >40–50 mm of meltwater release (T = 50–100 years) when the soil is frozen at least at the surface (T = 1–2 years) have a probability of only 1–2 % (Fig. 7; Table A.3). That said, the probability of a 2-year frost depth (>10 cm), co-occurring with a 2-year snowmelt event (>10 mm/d) or a 5-year snowmelt event (20 mm/d) is relatively high (joint probability of 28 % and 12 %). In contrast, rainfall during frost was found to have slightly larger event depths than those for snowmelt during frost, as well as marginally higher joint probabilities (joint probability of 30 % for a 2-year vs 2-year events; Fig. 7; Table A.3).

Table 6
Sensitivity analysis of selected soil and meteorological parameters.

Parameter	Properties	Soil temp.[1] [°C]	Max. frost depth [cm]	No. of days with frost	No. of FTCs
		RMSE, R^2	Max., Min, Avg. ± Std. Dev.		
Calibrated model run	Sandy loam, 10 cm grass	1.64, 0.92	39, 2.9, 15 ± 7	153, 26, 85 ± 30	8, 1, 4 ± 2
Soil texture	Loamy sand	1.60, 0.92	40, 1.7, 16 ± 9	147, 11, 78 ± 30	8, 1, 4 ± 2
	Loam	1.53, 0.93	38, 1.0, 13 ± 8	144, 9, 73 ± 31	9, 1, 4 ± 2
	Sandy clay loam	1.51, 0.93	38, 1.0, 12 ± 7	143, 9, 71 ± 31	9, 1, 4 ± 2
Vegetation cover	Bare ground	2.11, 0.91	38, 2, 16 ± 8	156, 27, 87 ± 31	9, 1, 4 ± 2
	5 cm	1.56, 0.92	38, 2, 15 ± 8	156, 25, 87 ± 30	8, 1, 4 ± 2
Hydraulic conductivity	1 cm/h	1.66, 0.92	37, 2, 15 ± 7	155, 26, 87 ± 30	8, 1, 4 ± 2
	10 cm/h	1.70, 0.92	37, 3, 16 ± 7	156, 30, 90 ± 30	9, 1, 4 ± 2
Precipitation corrected[2]	Snowfall	1.62, 0.92	37, 2, 15 ± 7	155, 23, 85 ± 30	8, 1, 4 ± 2

Notes: [1] Soil temperature simulated at 10 cm depth and compared with observations from 2007 to 2018 at the same depth. [2] Precipitation (snowfall) corrected for underestimated depth with wind speed.

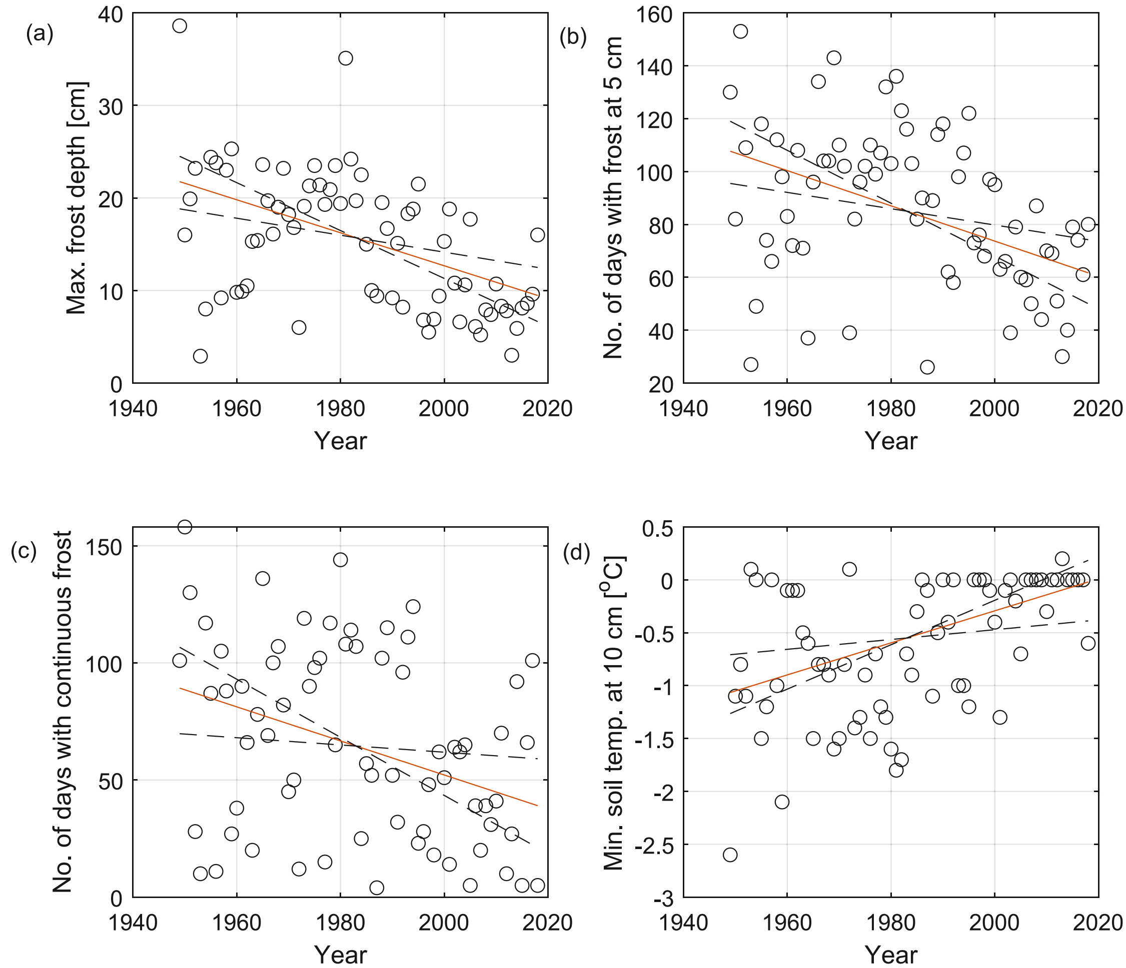

Fig. 6. a) maximum soil frost depth, b) number of days with soil frost at 5 cm depth, c) number of days with continuous frost, and d) minimum soil temperature at 10 cm depth in Reykjavík for the period of (1949–2018). The solid line represents Sen's slope, and the dashed lines represent the trend for the upper and lower 95 % confidence intervals of the slope.

Table 7
Median and trends of simulated soil conditions in Reykjavík 1949–2018.

Hydrological variable	Unit	Median	Sen's slope (unit/year)	R^2
Max. frost depth	cm	15.7	−0.18	0.24*
Soil frost at 5 cm depth	days	85.0	−0.67	0.15*
Soil frost at 15 cm depth	days	49.0	−0.84	0.18*
Continuous soil frost	days	64.5	−0.73	0.11^+
Min. soil temperature	°C	−0.55	0.015	0.23*

Notes: * $p < 0.001$, $^+ p < 0.01$

3.4. Timing of worst soil frost and runoff generation

Soil frost was most frequently simulated during peak winter months, from December to March (Fig. 8a). The 24-hour maximum frost depth in January and February was significantly higher than in the rest of the winter months (p-value < 0.05), with an average of 12.6 and 12.3 cm, respectively (Fig. 8b). This timing of maximum frost coincides very well with the largest RoS volume, averaging at 8.5, 9, and 11 mm in January, February, and March (Fig. 8c). The largest snowmelt depths also occurred in January and February (an average of 9.7 and 9.5 mm, respectively, Fig. 8d). Total precipitation and rainfall depth were highest during October, November, and December (not shown). The SHAW model predicts that the soil frost season has shortened significantly in

Table 8
Joint probability of occurrence during one year for the maximum RoS volume during the maximum frost depth for different return periods (T) during winter.

		Max. frost depth during RoS [cm]						
		0.7	11.2	19.5	25	29.4	35.1	39.1
Max. RoS volume during frost [mm]	T [years]	1	2	5	10	20	50	100
3.0	1	**0.977**	0.491	0.197	0.095	0.049	0.020	0.010
20.1	2	0.492	**0.266**	0.111	0.054	0.028	0.011	0.006
30.0	5	0.195	0.110	**0.047**	0.023	0.012	0.005	
35.4	10	0.099	0.056	0.024	**0.012**	0.006		
40.1	20	0.050	0.028	0.012	0.006			
45.5	50	0.020	0.011	0.005				
49.2	100	0.010	0.006					

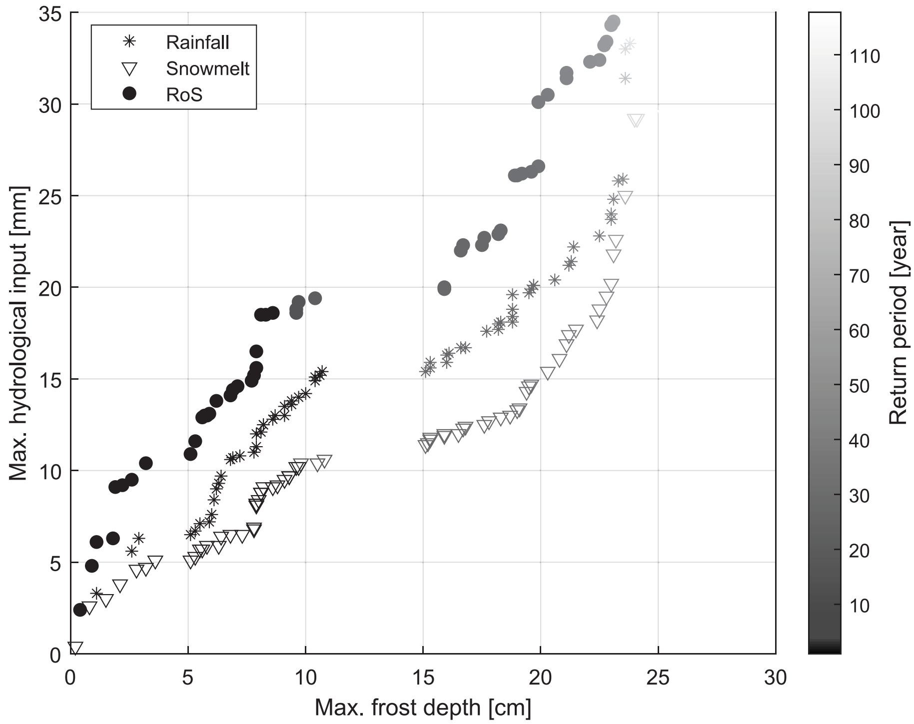

Fig. 7. The bivariate return periods for the hydrological inputs during frost are represented as snowmelt during frost, rainfall during frost, and RoS during frost.

the past 70 years, both with a delayed start (p-value > 0.05) and earlier end (p-value < 0.05; Fig. 9a and b, respectively). So, while the frost season is shortening, it is not affecting the likelihood of maximum frost co-occurring with maximum RoS. The fact that the last day of frost is no longer occurring as late as April and May suggests that the likelihood of maximum frost and maximum RoS or snowmelt occurring simultaneously may increase in the next few decades under continuous climate warming.

4. Discussion

This study focused on resolving the trends in soil frost and co-action with rain and snowmelt in a maritime climate undergoing frequent freeze–thaw cycles. With the help of a numerical, physically-based model, frost depth was found to decrease over the last 70 years under maritime climatic conditions, consistent with previous research (e.g., Nygren et al., 2021). The total number of frost days and duration of continuous frost decreased, suggesting shorter frost cycles, consistent with more intermittent frost. The number of freeze–thaw cycles also increased, but not at a significant level. This study also confirms previous research (e.g., Moghadas et al., 2018; Surfleet and Tullos, 2013) about the importance of RoS in generating urban floods: 24-hour RoS events were found to be on the order of 5 and 10 mm more voluminous than maximum rainfall and snowmelt events with the same return period (Fig. 7). However, the research adds to previous knowledge by highlighting that RoS-induced flood risk is connected to a high co-occurrence with soil frost. Mild rainfall and snowmelt events are known to result in significant damages if combined with deep frost formation, which can render the normally pervious areas during summer not conductive in winter (Bengtsson and Westerström, 1992; Westerström, 1984). At the studied site, even frost as shallow as 5 cm reduced the infiltration to a third of its summer rate in grassed surfaces and more in sparsely and non-vegetated areas (Zaqout et al., 2022). The results from this study also alleviated the uncertainties regarding the presence of soil frost in all major flooding events in Reykjavík during winter (Andradóttir et al., 2021).

While soil frost depth and duration were found to decrease in this study, which may ultimately suggest it is becoming a less relevant driver for urban flooding, there are no clear indications that winter floods will become more benign in the next decades. Conversely, the timing of maximum soil frost was found to shift so that it coincides more with the largest RoS and snowmelt events in the months of January–March. This, combined with a greater RoS volume, suggests that winter floods may intensify, at least in the next decades, while frost is still present. Urban areas transitioning from seasonal to intermittent snow covers may be particularly vulnerable to an increased risk of winter flooding. The repeated snowmelt during winter in conjunction with frequent freeze–thaw cycles are known to reduce soil insulation provided by an intact snow cover (Hardy et al., 2001; Moghadas et al., 2018). Consequently, deep frost formation that might be impervious until the thawing process is completed is expected to increase (Moghadas et al., 2018).

Winter conditions are often overlooked when designing drainage systems (Butler et al., 2018; Thorolfsson, 2012), as high-intensity, short-duration heavy summer rainfall is usually considered the largest cause of urban flooding (Bengtsson and Westerström, 1992; Hammond et al., 2015). Additionally, freeze–thaw cycles are often not taken into account in hydrological modeling (Qi et al., 2019), leading to an underestimation of runoff prediction. Since previous studies (e.g., Garvelmann et al., 2015; Surfleet and Tullos, 2013; Wever et al., 2014; Würzer and Jonas, 2018; Dong and Menzel, 2020; Ford et al., 2020) indicated that winter floods may become more voluminous and affect more regions with climate change, infiltration-inhibiting frost is still very relevant as found in this study. In light of these results, many urban areas may need to rethink their stormwater management practices, placing more emphasis

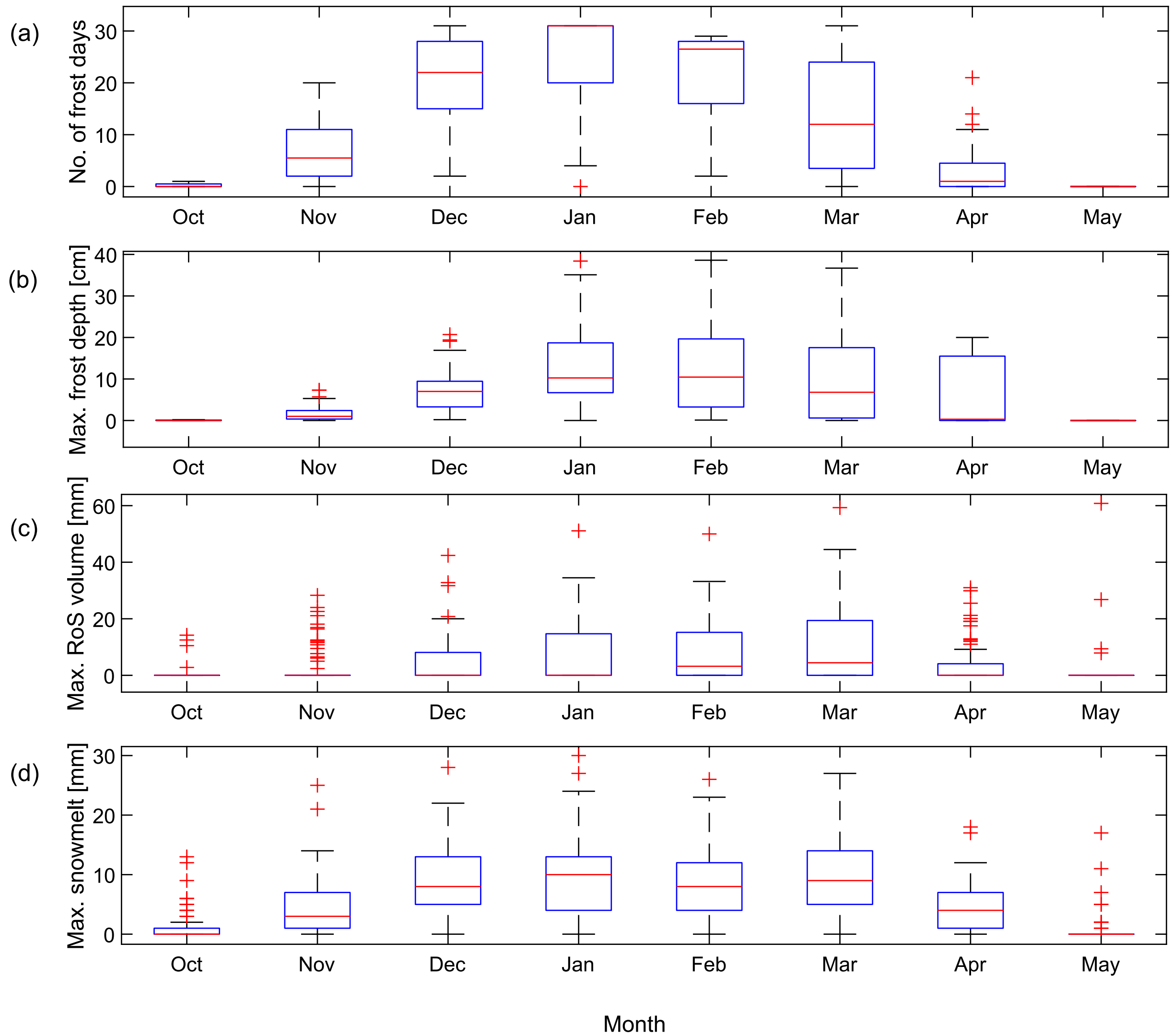

Fig. 8. A summary of the maximums of winter hydrological flood indicators per month for Reykjavík (1949–2018): a) no. of frost days, b) frost depth, c) RoS volume, and d) snowmelt. The whiskers extend to the maximum and minimum data points. Outliers are plotted individually as red crosses.

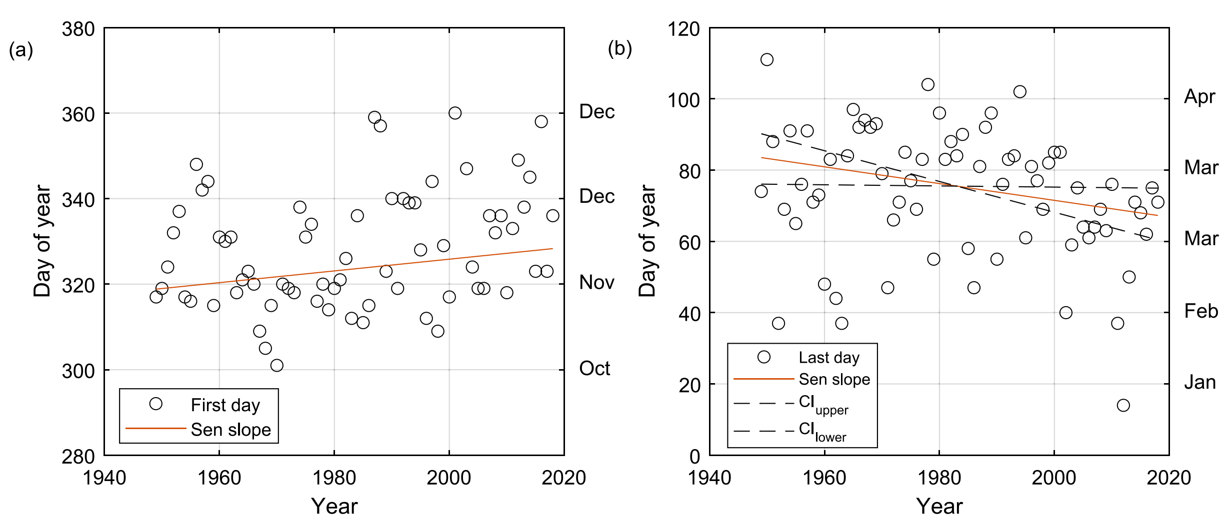

Fig. 9. Timing of beginning and end of soil freezing from 1949 to 2018 represented as a) trend in the first day of soil frost formation at the beginning of winter and b) trend in the last day of frost formation at the end of winter. The solid line represents Sen's slope, and the dashed lines represent the upper and lower confidence intervals of the significant slope.

on mitigating runoff augmentation because of infiltration inhibiting frost formation during frequent freeze–thaw. Infiltration-based sustainable urban drainage systems (SUDS) increase resilience to intensifying floods due to climate change as well as provide amenity, air quality and biodiversity benefits, which is in line with the United Nation's sustainable development goal no. 11 (https://sdgs.un.org). However, the risk of infiltration-inhibiting frost could be mitigated with the careful selection of soil, local vegetation, and the incorporation of underdrains (Caraco and Claytor, 1997; LeFevre et al., 2009; Roseen et al., 2009; Zaqout et al., 2022; Zaqout and Andradóttir, 2021).

This research highlights the importance of soil frost in winter urban hydrology and the role of numerical models in overcoming the lack of soil observations. The limitations in input data to the model were addressed systematically and comprehensively. The SHAW model was first tested on a site (Urriðaholt) with four years of detailed soil data. Then, the calibrated model was applied to a nearby site with limited data (Reykjavík). A selection of input parameters (i.e., the hydraulic conductivity, the saturated water content, and pore size index) were subsequently fine-tuned to increase the accuracy of simulations (RMSE $<$ 1.64 °C for the calibration period 2007–2018). Lastly, a sensitivity analysis was conducted to address the uncertainties in the input parameters and their influence on the key model outputs (i.e., maximum frost depth, number of frost days, and freeze–thaw cycles; Table 6). Soil texture and thermal properties influenced the accuracy of the model minimally, consistent with the results of Kahimba et al. (2009). This is because of counteracting mechanisms: On the one hand, fine-textured soils have a lower hydraulic conductivity compared to coarse-textured soils, which contributes to more frost formation during repeated freeze–thaw cycles (Zheng et al., 2021) and more surface runoff (Teng et al., 2020). On the other hand, fine soils have high thermal conductivity, so that they respond faster yet more moderately to changes in atmospheric heating and cooling because of their higher heat capacity as compared to their coarse counterparts (Lundin, 1990). The model simulations were somewhat sensitive to the type of vegetation cover, both the height of the grass canopy and density. Previous research also suggests that the root system can play an important role: A thick and dense root system has been shown to reduce the thermal conductivity of the underlying soil (Yang et al., 2005), consistent with grass cover being less susceptible to frost formation, soil deformation, and freeze–thaw cycles than less vegetated or barren areas (Zaqout et al., 2022). In this study, the model overestimated the soil temperature and underestimated frost formation during winter in Reykjavík, which could reflect a less extensive vegetation cover than assumed. In general, the model results agreed well with the measured hourly observations at both tested sites and the simulated soil temperature was not negatively affected by the inaccuracies in soil moisture prediction (Table 4). This was specifically true for the Urriðaholt site with deviations of $<$1.0 °C at all simulation depths, which indicates good agreement with measured values (Eitzinger et al., 2000). The model showed little sensitivity to variations in calibration parameters in the Reykjavík study site as R^2 ranged between 0.91 and 0.93 for all tested parameters. Lastly, the historical predictions were conducted on daily time-step basis, and as such, precipitation was classified as either in liquid or dry form based on air temperature and relative humidity for each day (Eq. (11)). This simplification does not affect the major results of the study, which focused either on long term averages, or annual maximum hydrological events.

5. Conclusions

In this paper, soil temperature, liquid and ice moisture content, and frost depth were simulated for two study areas in the greater capital region of Iceland using the Simultaneous Heat and Water (SHAW) model. A good agreement between the simulated and observed data was found at the two tested sites ($R^2 > 0.91$), which provided valuable insights into the freezing and thawing processes. The numerical model proved particularly helpful in overcoming the lack of the long-term soil observations needed for frequency and trend analyses and resolving very shallow frost that is difficult to measure (within the top 5 cm). The results show that the rise in air temperatures and liquid precipitation in winter due to climate change resulted in a significant reduction in frost depth over the last 70 years. However, a shift in the timing of maximum frost depth occurred and started to coincide with the largest winter events, which might pose a higher urban flood risk in the future if the trend continues. This study highlights the importance of analyzing the co-acting hydrologic variables, which is specifically needed in a cold climate, as severe events can result from two mundane events happening simultaneously, especially in the presence of soil frost that is often overlooked in the design of urban drainage systems. In particular, rain-on-snow events during frost were found to pose the greatest flood risk, being more voluminous than rainfall or snowmelt alone. The changing winter patterns and hydrological processes require a reconsideration of the planning and design of urban drainage systems, specifically due to the increase in the number, frequency, and magnitude of rain-on-snow events in the last decades. Therefore, a shift towards more sustainable approaches for stormwater management and re-thinking urban runoff generation and drainage systems from a single-variate, single-purpose approach to a multipurpose approach is urged.

Declaration of Competing Interest

The authors declare that they have no known competing financial interests or personal relationships that could have appeared to influence the work reported in this paper.

Data availability

The data used in this study were collected from the field by the researchers and acquired from the Icelandic Meteorological Office (IMO). Any additional data is available upon request from the aforementioned rightful owners.

Acknowledgments

This research was funded by the Icelandic Research Fund (Icelandic: Rannís), grant number 185398-053. We thank the Garðabær Municipality, Iceland Meteorological Office, and Urriðaholt ehf for on-site research facilities. The Agricultural University of Iceland, especially to Prof. Ólafur Arnalds for his valuable soil insights. Viðar Guðmundsson, professor in Physics at the University of Iceland, is thanked for his help with programming. A special thanks goes to Halldóra Hreggviðsdóttir for motivating and facilitating SUDS research in Iceland.

Appendix

The bivariate Archimedean copula family fitted to each pair of annual maximum hydrological variables (i.e., snowmelt & frost, rainfall & frost, and RoS & frost) was chosen based on the highest log-likelihood and lowest AIC and BIC, which are highlighted in Table A.1. The parameter of each bivariate copula was estimated using the maximum likelihood method (Table A.1).

The joint probability of maximum snowmelt occurring with maximum frost and the maximum rainfall occurring with maximum frost are shown in Table A.3. The highlighted joint probabilities indicate the events of interest for return periods $1 < T < 100$ years.

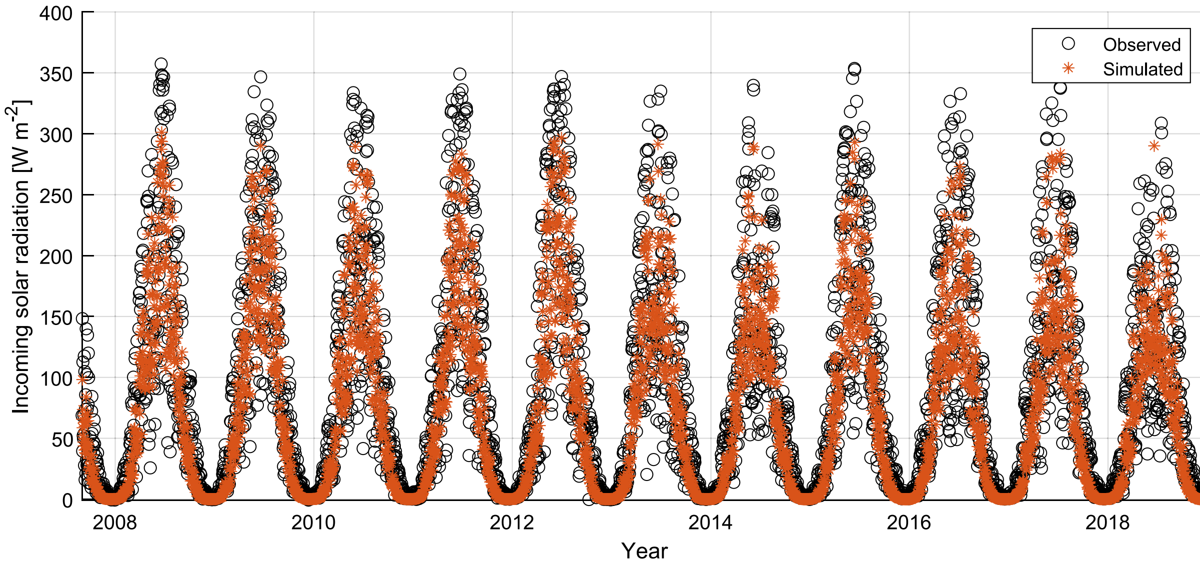

Fig. A1. Measured and simulated incoming daily solar radiation in Reykjavík for the period of 2007–2018.

Table A1
Copula parameter estimation and selection criteria of copula model.

	Family	θ	Kendall's tau	Selection criteria		
				Log-Likelihood	AIC	BIC
Snowmelt during frost	Clayton	0.33	0.14	**1.92**	**−1.85**	**0.40**
	Gumbel	1.13	0.11	0.84	0.32	2.57
	Joe	1.13	0.07	0.38	1.25	3.50
	Frank	1.08	0.12	1.04	−0.09	2.16
Rainfall during frost	Clayton	0.52	0.21	**4.47**	**−6.94**	**4.69**
	Gumbel	1.18	0.15	1.50	−0.99	1.25
	Joe	1.14	0.07	0.33	1.34	3.59
	Frank	1.85	0.20	3.11	−4.22	−1.97
RoS during frost	Clayton	0	0	0	2.00	4.01
	Gumbel	1.04	0.04	0.06	1.87	3.88
	Joe	1.06	0.03	0.06	1.88	3.89
	Frank	0.62	0.07	**0.27**	**1.46**	**3.47**

Table A2
Goodness of fit test statistic for distribution selection, and parameter estimation for the marginal distributions using maximum likelihood method.

	Distribution	Goodness-of-fit			Selection criteria		Parameter estimation		
		Kolmogorov-Smirnov	Cramer-von Mises	Anderson-Darling	AIC	BIC		μ/β	σ/η
Max. Snowmelt during frost [mm]	Lognormal	0.104	0.152	0.967	480.7	485.2	Estimate	2.34	0.70
							Std. Error	0.08	0.06
Max. Frost depth during snowmelt [cm]	Weibull	0.125	0.194	1.074	487.5	492.0	Estimate	1.68	15.3
							Std. Error	0.16	1.14
Max. Rainfall during frost [mm]	Lognormal	0.069	0.064	0.388	483.9	488.4	Estimate	2.73	0.49
							Std. Error	0.06	0.04
Max. Frost depth during rainfall [cm]	Weibull	0.120	0.240	1.281	480.5	485.0	Estimate	1.97	16.37
							Std. Error	0.19	1.05
Max. RoS volume during frost [mm]	Weibull	0.064	0.041	0.293	413.1	417.2	Estimate	2.11	23.81
							Std. Error	0.22	1.61
Max. frost depth during RoS [cm]	Weibull	0.168	0.238	1.376	383.6	387.7	Estimate	1.51	14.18
							Std. Error	0.17	1.33

Table A3
Joint probability of occurrence for the annual maxima of the hydrological variables for different return periods during winter.

		Max. frost depth during snowmelt [cm]						
		1.1	12.3	20.3	25.2	29.3	34.3	37.8
Max. snowmelt during frost [mm]	T [years]	1	2	5	10	20	50	100
2.0	1	**0.981**	0.498	0.198	0.098	0.050	0.020	0.010
10.4	2	0.498	**0.284**	0.117	0.058	0.030	0.012	0.006
18.8	5	0.199	0.118	**0.050**	0.025	0.013	0.005	
25.5	10	0.100	0.059	0.025	**0.013**	0.006		

(*continued on next page*)

Table A3 (*continued*)

		Max. frost depth during snowmelt [cm]						
		1.1	12.3	20.3	25.2	29.3	34.3	37.8
32.9	20	0.050	0.030	0.013	0.006			
43.9	50	0.020	0.012	0.005				
53.1	100	0.010	0.006					
		Max. frost depth during rainfall [cm]						
		1.7	13.5	21.0	25.2	28.5	32.7	35.5
Max. rainfall during frost [mm]	T [years]	1	2	5	10	20	50	100
5.0	1	**0.981**	0.504	0.195	0.096	0.051	0.020	0.010
15.2	2	0.503	**0.305**	0.125	0.062	0.033	0.013	0.007
23.1	5	0.198	0.127	**0.053**	0.027	0.014	0.006	
28.3	10	0.103	0.067	0.028	**0.014**	0.008		
34.0	20	0.050	0.033	0.014	0.007			
41.6	50	0.020	0.013	0.006				
47.5	100	0.010	0.007					

References

Andradóttir, H.Ó., Arnardóttir, A.R., Zaqout, T., 2021. Rain on snow induced urban floods in cold maritime climate: Risk, indicators and trends. Hydrol. Process. 35 (9), e14298.

Arnalds, O., 2015. The Soils of Iceland. Springer, Netherlands. https://doi.org/10.1007/978-94-017-9621-7.

Bengtsson, L., Westerström, G., 1992. Urban snowmelt and runoff in northern Sweden. Hydrol. Sci. J. 37 (3), 263–275. https://doi.org/10.1080/02626669209492586.

Benninghoff, W.S., 1952. Interaction of vegetation and soil frost phenomena. Arctic 5 (1), 34–44.

Bras, R.L., 1990. Hydrology: An Introduction to Hydrologic Science. Addison-Wesley.

Butler, D., Digman, C., Makropoulos, C., & Davies, J. W. (2018). *Urban Drainage* (4th ed.). CRC Press. 10.1201/9781351174305.

Campbell, G.S., 1974. A simple method for determining unsaturated conductivity from moisture retention data. Soil Sci. 117 (6), 311–314.

Caraco, D., Claytor, R., 1997. Stormwater BMP Design: Supplement for Cold Climates. Environmental Protection Agency, U.S.

Chen, L. (2019). *Copulas and Its Application in Hydrology and Water Resources / by Lu Chen, Shenglian Guo.* (1st ed. 2019.). Springer Singapore. 10.1007/978-981-13-0574-0.

Chow, V.T., Maidment, D.R., Mays, L.W., 1988. Applied Hydrology. McGraw-Hill.

Clayton, D.G., 1978. A model for association in bivariate life tables and its application in epidemiological studies of familial tendency in chronic disease incidence. Biometrika 65 (1), 141–151. https://doi.org/10.1093/biomet/65.1.141.

Crochet, P., Jóhannesson, T., Jónsson, T., Sigurðsson, O., Björnsson, H., Pálsson, F., Barstad, I., 2007. Estimating the spatial distribution of precipitation in iceland using a linear model of orographic precipitation. J. Hydrometeorol. 8 (6), 1285–1306. https://doi.org/10.1175/2007JHM795.1.

de Vries, D.A., 1963. Thermal properties of soils. In: van Wijk, W.R. (Ed.), Physics of Plant Environment, (2nd ed.,. North Holland Publishing Company, pp. 210–235.

Dong, C., Menzel, L., 2020. Recent snow cover changes over central European low mountain ranges. Hydrol. Process. 34 (2), 321–338. https://doi.org/10.1002/hyp.13586.

Einarsson, M., 1984. Climate of Iceland. Elsevier.

Eitzinger, J., Parton, W., Hartman, M., 2000. Improvement and validation of a daily soil temperature submodel for freezing/thawing periods. Soil Sci. 165, 525–534. https://doi.org/10.1097/00010694-200007000-00001.

Kahimba, F., Sri Ranjan, R., & Mann, D. (2009). Modeling Soil Temperature, Frost Depth, and Soil Moisture Redistribution in Seasonally Frozen Agricultural Soils. *Applied Engineering in Agriculture*, *25*, 871–882. 10.13031/2013.29237.

Feiccabrino, J., Graff, W., Lundberg, A., Sandström, N., Gustafsson, D., 2015. Meteorological knowledge useful for the improvement of snow rain separation in surface based models. Hydrology 2 (4), 266–288. https://doi.org/10.3390/hydrology2040266.

Flerchinger, G., 2000. The Simultaneous Heat and Water (SHAW). Technical Documentation, Model.

Flerchinger, G.N., Pierson, F.B., 1991. Modeling plant canopy effects on variability of soil temperature and water. Agric. For. Meteorol. 56 (3), 227–246. https://doi.org/10.1016/0168-1923(91)90093-6.

Ford, C.M., Kendall, A.D., Hyndman, D.W., 2020. Effects of shifting snowmelt regimes on the hydrology of non-alpine temperate landscapes. J. Hydrol. 590, 125517 https://doi.org/10.1016/j.jhydrol.2020.125517.

Fouli, Y., Cade-Menun, B.J., Cutforth, H.W., 2013. Freeze–thaw cycles and soil water content effects on infiltration rate of three Saskatchewan soils. Can. J. Soil Sci. 93 (4), 485–496. https://doi.org/10.4141/cjss2012-060.

Frank, M.J., 1979. On the simultaneous associativity ofF(x, y) andx+y−F(x, y). Aequationes Math. 19 (1), 194–226. https://doi.org/10.1007/BF02189866.

Fuchs, M., Campbell, G.S., Papendick, R.I., 1978. An analysis of sensible and latent heat flow in a partially frozen unsaturated soil. Soil Sci. Soc. Am. J. 42 (3), 379–385. https://doi.org/10.2136/sssaj1978.03615995004200030001x.

Flerchinger, G., & Saxton, K. (1989a). Simultaneous Heat and Water Model of a Freezing Snow-Residue-Soil System I. Theory and Development. *Transactions of the ASAE*, *32*, 0565–0571. 10.13031/2013.31040.

Flerchinger, G., & Saxton, K. (1989b). Simultaneous Heat and Water Model of a Freezing Snow-Residue-Soil System II. Field verification. *Transactions of the ASAE*, *32*, 0573–0576. 10.13031/2013.31041.

Garvelmann, J., Pohl, S., Weiler, M., 2015. Spatio-temporal controls of snowmelt and runoff generation during rain-on-snow events in a mid-latitude mountain catchment. Hydrol. Process. 29 (17), 3649–3664. https://doi.org/10.1002/hyp.10460.

Gilbert, R.O., 1987. Statistical Methods for Environmental Pollution Monitoring (1st edition). Wiley.

Granger, R., Gray, D., Dyck, G., 2011. Snowmelt infiltration to frozen prairie soils. Can. J. Earth Sci. 21, 669–677. https://doi.org/10.1139/e84-073.

Gumbel, E.J., 1960. Bivariate exponential distributions. J. Am. Stat. Assoc. 55 (292), 698–707.

Guymon, G.L., Luthin, J.N., 1974. A coupled heat and moisture transport model for Arctic soils. Water Resour. Res. 10 (5), 995–1001. https://doi.org/10.1029/WR010i005p00995.

Hammond, M.J., Chen, A.S., Djordjević, S., Butler, D., Mark, O., 2015. Urban flood impact assessment: A state-of-the-art review. Urban Water J. 12 (1), 14–29. https://doi.org/10.1080/1573062X.2013.857421.

Hansson, K., Šimůnek, J., Mizoguchi, M., Lundin, L.-C., van Genuchten, M.T., 2004. Water flow and heat transport in frozen soil: Numerical solution and freeze-thaw applications. Vadose Zone J. 3 (2), 693–704. https://doi.org/10.2136/vzj2004.0693.

Hardy, J.P., Groffman, P.M., Fitzhugh, R.D., Henry, K.S., Welman, A.T., Demers, J.D., Fahey, T.J., Driscoll, C.T., Tierney, G.L., Nolan, S., 2001. Snow depth manipulation and its influence on soil frost and water dynamics in a northern hardwood forest. Biogeochemistry 56 (2), 151–174. https://doi.org/10.1023/A:1013036803050.

He, H., Dyck, M.F., Si, B.C., Zhang, T., Lv, J., Wang, J., 2015. Soil freezing–thawing characteristics and snowmelt infiltration in Cryalfs of Alberta, Canada. Geoderma Reg. 5, 198–208. https://doi.org/10.1016/j.geodrs.2015.08.001.

Jansson, P.-E., Karlberg, L., 2004. Coupled heat and mass transfer model for soil-plant-atmosphere systems. Stockholm, Royal Institute of Technology, Department of Civil and Environmental Engineering.

Joe, H., 1997. Multivariate Models and Multivariate Dependence Concepts. CRC Press.

Kane, D.L., 1980. Snowmelt infiltration into seasonally frozen soils. Cold Reg. Sci. Technol. 3 (2–3), 153–161. https://doi.org/10.1016/0165-232X(80)90020-8.

Kendall, M.G., 1948. Rank correlation methods. Griffin.

Khan, U.T., Valeo, C., Chu, A., van Duin, B., 2012. Bioretention cell efficacy in cold climates: Part 1 — hydrologic performance. Can. J. Civ. Eng. 39 (11), 1210–1221. https://doi.org/10.1139/l2012-110.

LeFevre, N.J., Davidson, J.D., Oberts, G.L., 2009. Bioretention of simulated Snowmelt: Cold climate performance and design criteria. Cold Regions Eng. 2009, 145–154. https://doi.org/10.1061/41072(359)17.

Lian, J., Xu, K., Ma, C., 2013. Joint impact of rainfall and tidal level on flood risk in a coastal city with a complex river network: A case study of Fuzhou City, China. Hydrol. Earth Syst. Sci. 17, 679–689. https://doi.org/10.5194/hess-17-679-2013.

Lundin, L.-C., 1990. Hydraulic properties in an operational model of frozen soil. J. Hydrol. 118 (1), 289–310. https://doi.org/10.1016/0022-1694(90)90264-X.

Maksimovic, C., Saegrov, S., Milina, J., & Thorolfsson, S. (2000). *Urban drainage in specific climates, v. II: Urban drainage in cold climates—UNESCO Digital Library*. https://unesdoc.unesco.org/ark:/48223/pf0000122599.

Mann, H.B., 1945. Nonparametric tests against trend. Econometrica 13 (3), 245.

Moghadas, S., Leonhardt, G., Marsalek, J., Viklander, M., 2018. Modeling urban runoff from rain-on-snow events with the U.S. EPA SWMM model for current and future climate scenarios. J. Cold Reg. Eng. 32 (1), 04017021. https://doi.org/10.1061/(ASCE)CR.1943-5495.0000147.

Muthanna, T.M., Viklander, M., Thorolfsson, S.T., 2008. Seasonal climatic effects on the hydrology of a rain garden. Hydrol. Process. 22 (11), 1640–1649. https://doi.org/10.1002/hyp.6732.

Nelsen, R.B., 2007. An Introduction to Copulas. Springer Science & Business Media.

Nygren, M., Giese, M., Barthel, R., 2021. Recent trends in hydroclimate and groundwater levels in a region with seasonal frost cover. J. Hydrol. 602, 126732 https://doi.org/10.1016/j.jhydrol.2021.126732.

Iceland Meteorological Office [IMO] (2020b). Daily weather observations at the Reykjavík Manned Synoptic Station No. 1.

Iceland Meteorological Office [IMO] (2022a). Incoming and outgoing radiation from Reykjavik station No. 7476. Data delivery May 11, 2022.
Ólafsson, H., Furger, M., Brümmer, B., 2007. The weather and climate of Iceland. Meteorologische Zeitschrift - METEOROL Z 16 (1), 5–8.
Penner, E., 1970. Thermal conductivity of frozen soils. Can. J. Earth Sci. 7 (3), 982–987.
Petersen, G.N., 2018. Veður í Reykjavík og á Hólmsheiði Desember 2017 – Janúar 2018. Orkuveita Reykjavíkur. Technical Report GNP/2018-1,.
Qi, J., Zhang, X., Wang, Q., 2019. Improving hydrological simulation in the Upper Mississippi River Basin through enhanced freeze-thaw cycle representation. J. Hydrol. 571, 605–618. https://doi.org/10.1016/j.jhydrol.2019.02.020.
Roseen, R.M., Ballestero, T.P., Houle, J.J., Avellaneda, P., Briggs, J., Fowler, G., Wildey, R., 2009. Seasonal performance variations for storm-water management systems in cold climate conditions. J. Environ. Eng. 135 (3), 128–137. https://doi.org/10.1061/(ASCE)0733-9372(2009)135:3(128).
Salvadori, G., De Michele, C., 2007. On the use of copulas in hydrology: Theory and practice. J. Hydrol. Eng. 12 (4), 369–380. https://doi.org/10.1061/(ASCE)1084-0699(2007)12:4(369).
Sen, P.K., 1968. Estimates of the regression coefficient based on Kendall's Tau. J. Am. Stat. Assoc. 63 (324), 1379–1389. https://doi.org/10.2307/2285891. JSTOR.
Shanley, J.B., Chalmers, A., 1999. The effect of frozen soil on snowmelt runoff at Sleepers River, Vermont. Hydrol. Process. 13 (12–13), 1843–1857. https://doi.org/10.1002/(SICI)1099-1085(199909)13:12/13<1843::AID-HYP879>3.0.CO;2-G.
Šimůnek, J., van Genuchten, M. Th., & Šejna, M. (2016). Recent Developments and Applications of the HYDRUS Computer Software Packages. *Vadose Zone Journal*, *15* (7), vzj2016.04.0033. 10.2136/vzj2016.04.0033.
Sklar, M., 1959. Fonctions de repartition a n dimensions et leurs marges. Undefined. https://www.semanticscholar.org/paper/Fonctions-de-repartition-a-n-dimensions-et-leurs-Sklar/d017e0a6a9b93dcab7cdcd44b17544c04f7678d2.
Slater, A.G., Pitman, A.J., Desborough, C.E., 1998. Simulation of freeze-thaw cycles in a general circulation model land surface scheme. J. Geophys. Res. 103 (D10), 11303–11312.
Sörensen, J., & Bengtsson, L. (2014). *Combined effects of high water level and precipitation on flooding of Gothenburg, Sweden* (p. 12).
Stadler, D., Stahli, M., Aeby, P., Fluhler, H., 2000. Dye tracing and image analysis for quantifying water infiltration into frozen soils. Soil Sci. Soc. Am. J. 64 (2), 505–516. https://doi.org/10.2136/sssaj2000.642505x.
Stähli, M., Jansson, P.-E., Lundin, L.-C., 1999. Soil moisture redistribution and infiltration in frozen sandy soils. Water Resour. Res. 35 (1), 95–103. https://doi.org/10.1029/1998WR900045.
Surfleet, C.G., Tullos, D., 2013. Variability in effect of climate change on rain-on-snow peak flow events in a temperate climate. J. Hydrol. 479, 24–34. https://doi.org/10.1016/j.jhydrol.2012.11.021.
Teng, J., Kou, J., Yan, X., Zhang, S., Sheng, D., 2020. Parameterization of soil freezing characteristic curve for unsaturated soils. Cold Reg. Sci. Technol. 170, 102928 https://doi.org/10.1016/j.coldregions.2019.102928.
Theil, H., 1950. A rank-invariant method of linear and polynomial regression analysis, 1–2; confidence regions for the parameters of linear regression equations in two, three and more variables. Indag. Math. 1 (2). https://ir.cwi.nl/pub/18446.
Thorolfsson, S. T. (2012). *Specific Problems in Urban Drainage in Cold Climate (SP-UDCC)*. 888–899. 10.1061/40583(275)86.
Usda, 1987. Soil Mechanics Level 1: Module 3—USDA Textural Soil Classification. Study Guide.
Wang, G., Hu, H., Li, T., 2009. The influence of freeze–thaw cycles of active soil layer on surface runoff in a permafrost watershed. J. Hydrol. 375 (3), 438–449. https://doi.org/10.1016/j.jhydrol.2009.06.046.
Watanabe, K., Kito, T., Dun, S., Wu, J. Q., Greer, R. C., & Flury, M. (2013). Water Infiltration into a Frozen Soil with Simultaneous Melting of the Frozen Layer. *Vadose Zone Journal*, *12*(1), vzj2011.0188. 10.2136/vzj2011.0188.
Watanabe, K., Kugisaki, Y., 2017. Effect of macropores on soil freezing and thawing with infiltration: Effect of Macropores on Soil Freezing and Thawing with Infiltration. Hydrol. Process. 31 (2), 270–278. https://doi.org/10.1002/hyp.10939.
Westerström, G., 1984. Snowmelt runoff from Porsön residential area. Luleå. 4, 315–323. http://urn.kb.se/resolve?urn=urn:nbn:se:ltu:diva-38161.
Wever, N., Jonas, T., Fierz, C., Lehning, M., 2014. Model simulations of the modulating effect of the snow cover in a rain-on-snow event. Hydrol. Earth Syst. Sci. 18 (11), 4657–4669. https://doi.org/10.5194/hess-18-4657-2014.
Williams, P.J., Smith, M.W., 1989. The frozen earth: Fundamentals of geocryology, Vol. 306. Cambridge University Press Cambridge.
Würzer, S., Jonas, T., 2018. Spatio-temporal aspects of snowpack runoff formation during rain on snow. Hydrol. Process. 32 (23), 3434–3445. https://doi.org/10.1002/hyp.13240.
Würzer, S., Jonas, T., Wever, N., Lehning, M., 2016. Influence of initial snowpack properties on runoff formation during rain-on-snow events. J. Hydrometeorol. 17 (6), 1801–1815. https://doi.org/10.1175/JHM-D-15-0181.1.
Yang, K., Koike, T., Ye, B., Bastidas, L., 2005. Inverse analysis of the role of soil vertical heterogeneity in controlling surface soil state and energy partition. J. Geophys. Res. Atmos. 110 (D8) https://doi.org/10.1029/2004JD005500.
Zaqout, T., Andradóttir, H.Ó., 2021. Hydrologic performance of grass swales in cold maritime climates: Impacts of frost, rain-on-snow and snow cover on flow and volume reduction. J. Hydrol. 597, 126159 https://doi.org/10.1016/j.jhydrol.2021.126159.
Zaqout, T., Andradóttir, H.Ó., Arnalds, Ó., 2022. Infiltration capacity in urban areas undergoing frequent snow and freeze–thaw cycles: Implications on sustainable urban drainage systems. J. Hydrol. 607, 127495 https://doi.org/10.1016/j.jhydrol.2022.127495.
Zellou, B., Rahali, H., 2019. Assessment of the joint impact of extreme rainfall and storm surge on the risk of flooding in a coastal area. J. Hydrol. 569, 647–665. https://doi.org/10.1016/j.jhydrol.2018.12.028.
Zheng, C., Šimůnek, J., Zhao, Y., Lu, Y., Liu, X., Shi, C., Li, H., Yu, L., Zeng, Y., Su, Z., 2021. Development of the Hydrus-1D freezing module and its application in simulating the coupled movement of water, vapor, and heat. J. Hydrol. 598, 126250 https://doi.org/10.1016/j.jhydrol.2021.126250.